Frontiers in Heat and Mass Transfer (FHMT), 1, 023007 (2010)
DOI: 10.5098/hmt.v1.2.3007

Global Digital Central
ISSN: 2151-8629

Frontiers in Heat and Mass Transfer

Available at www.ThermalFluidsCentral.org

EXPERIMENTAL STUDY OF ENHANCED NUCLEATE BOILING HEAT TRANSFER ON UNIFORM AND MODULATED POROUS STRUCTURES

Calvin Hong Li [a] and G. P. Peterson[b,*]

[a] *Department of Mechanical, Industrial, and Manufacturing Engineering, University of Toledo, Toledo, Ohio, 43606, USA*
[b] *G.W. Woodruff School of Mechanical Engineering, Georgia Institute of Technology, Atlanta, Georgia 30332, USA*

ABSTRACT

An experimental investigation of the Critical Heat Flux (CHF) and heat transfer coefficient (HTC) of two-phase heat transfer of de-Ionized (DI) water, pool boiling was conducted using several kinds of sintered copper microparticle porous uniform and modulated structures. The modulated porous structure reached a heat flux of 450 W/cm^2 and a heat transfer coefficient of 230,000 W/m^{2}K. The thick and thin uniform porous structures achieved CHFs of 290 W/cm^2 and 227 W/cm^2, respectively, and heat transfer coefficients of 118,000 W/m^{2}K and 104,000 W/m^{2}K. The mechanisms for the dramatically improved CHFs and HTCs were identified with assistance of a visualization study.

Keywords: *pool boiling, surface modification, contact angle, hydrodynamic instability, CHF.*

1. INTRODUCTION

High capacity heat transfer techniques are necessary in a wide range of modern industrial processes and scientific investigations, including concentrated solar conversion technologies, laser generator cooling, and high performance thermal management systems. It has long been recognized that two-phase heat transfer processes have greater heat transfer capability than conventional single phase convection using either air or water. This is the result of the high latent heat of the working fluid and is of particular significance in ultra high heat flux applications. As a result, two-phase heat transfer techniques have been widely adopted in many thermal management frontiers (Peterson, 1994). However, broader applications of two-phase heat transfer are constrained by the CHF which is a critical issue in these two-phase heat transfer applications.

In some of the earliest studies of the effect of surface roughness on pool boiling CHF and the heat transfer coefficients of n-pentane, there was clear indication that the pool boiling heat transfer coefficient could be improved by as much as 600% by simply modifying the surface roughness (Zhao et al., 1998). As a result, a number of researchers have devoted considerable effort to identify the relationship between this increased pool boiling heat transfer and the physical characteristics of the modified heating surfaces. Intensive research in pool boiling heat transfer has shown that enhanced heating surface structures could lead to significant improvements in CHF and heat transfer coefficient (Faghri, 1995 and Berenson, 1962). Among those enhanced surface structures studied are plain surfaces with re-entrant cavities, finned surfaces, and surfaces with various shaped channels. Other kinds of surface structures that have been studied extensively are porous structures that use sintered or soldered metal particles, sintered metal wire, or metal foam. Research in porous structure coated heating surfaces, has demonstrated great promise in the possible improvement of both the CHF and the heat transfer coefficient.

A surface is assumed to reach the CHF when the hydrodynamic instability limit is reached for a particular application. By reducing the vapor bubble departure size and/or separating the adjacent vapor columns, it is possible to delay the onset of this hydrodynamic instability, and in turn, the onset of CHF. Additionally, porous structure coatings on a heated surface will increase the bubble nucleation site density, which could also improve the rate of liquid vaporization, thereby improving the heat transfer coefficient, particularly at the early stage of nucleate pool boiling. Moreover, the capillary forces generated in these porous structure coatings could retard the onset of dry-out of the heated surface. At the late stage of pool boiling, the modulated porous structure will improve the CHF by delaying the occurrence of hydrodynamic instability (Li et al., 2009 and Li, 2009).

This delayed occurrence of hydrodynamic instability by these structures has been studied in several investigations. Kaviany et al. (2001, 2006, and 2009) analytically and experimentally investigated the characteristics of pool boiling on modulated and uniform porous structures using pentane as the working fluid. The geometry of the porous media and the particle size used in the porous media, was specifically designed according to the physical properties of pentane. The results indicate that the CHF can be dramatically improved, on both modulated and uniform structures, with the modulated structure exhibiting superior performance over the uniform structure. The authors attribute this to the fact that modulated porous structure effectively separates the liquid phase flow and vapor phase flow, thereby reducing the liquid-vapor counterflow resistance near the heated surface. This reduced counterflow resistance leads to the delayed onset of the

* *Corresponding author. Email: Bud.peterson@gatech.edu*

DOI: 10.5098/hmt.v1.2.3007 ISSN: 2151-8629

hydrodynamic instability. As the distance between the two adjacent conical stacks is optimized for the liquid-vapor counterflow, the hydrodynamic liquid choking limit is increased, and the CHF follows suit.

Connor and You (1995) improved the two phase heat transfer performance of an aluminum foil heating surface by painting a silver microstructure coating on the top of the foil. The thickness of the silver coating was approximately 25μm with a cavity size of 1 μm. FC-72 was used as the working fluid in this study. The visualization results showed that smaller departing bubbles (diameter 0.6 to 1.0 mm) were generated compared to what occurred on plain surfaces. Experimental results also demonstrated a significant improvement in the CHF, which reached 30 W/cm^2, twice the CHF value obtained using aluminum foil without the top silver coating. The superheat values were between 6ºC to 10ºC which was 70%-85% less than that obtained for a plain surface under the same heating conditions. The hypothesis proposed was that that the microstructure of the aluminum foil with the silver coating significantly changed the bubble behavior, which resulted in the two phase heat transfer performance improvement.

Chang and You (1997) continued to experimentally investigate the FC-72 two phase nucleate boiling on both diamond microporous coatings (Diamond particle sizes are 2, 10 and 20 μm and the coating thicknesses are 30, 50 and 100 μm, respectively) and large porous size coatings (diamond particle sizes are 45 and 70 μm, and the coating thicknesses are 200 and 250 μm) on a flat copper surface. It was found that the large porous size coating demonstrated a better heat transfer performance at a low heat flux due to increased active nucleation sit density, but when the heat flux was over 2.5 W/cm^2, the microporous coatings illustrated a better performance surpassing large porous coatings. It is explained that, due to the larger porous size coating have a higher impedance for liquid-vapor exchange channels and a higher thermal resistance, the two phase heat transfer performance will be worse in larger porous size structures at the higher heat fluxes. However, the CHF reached 28 W/cm^2 for the larger porous size structure, while CHF was 26 W/cm^2 for the microporous surface. Under the same heating situation, the CHF on a plain surface was only 14 W/cm^2.

Rainey and You (2000) performed boiling experiments on pin-finned surfaces with a microporous media coating in a saturated FC-72 fluid. It is reported that the incipient superheat has been reduced from 25-40 K down to less than 10 K with the increased surface roughness with the microporous coating. The heat transfer coefficient was also dramatically increased, for example, at 10 W/cm^2 heat flux, the heat transfer coefficient of the microporous roughened surface exhibited 300 % increase over that of a polished surface. The thermal performance improvement was the result of surface area enhancement, fin efficiency, surface microstructure, reduction of vapor bubble departure resistance, and re-wetting liquid flow resistance.

Vemuri and Kim (2005) experimentally investigated the boiling heat transfer characteristics of nano-porous surfaces made of aluminum oxide with a thickness of 70 μm using FC-72 as the working fluid. The superheat was reduced by 30% at the same heat flux compared to that of a plain aluminum oxide surface. The reduced superheat was attributed to the fact that the nano-scale pores increased both the vapor entrapment volume and the active nucleation site density, which as shown previously, greatly enhances the two phase heat transfer performance.

Melendez and Reyes (2006) conducted a series of experiments using a positive binary mixture, boiling on porous coverings made of iron wool and stainless steel wool. It was observed that bubble size and bubble coalescence were reduced while fluid replenishment was increased during the process of two phase heat transfer when the porosity increased. The reduced size of bubble and bubble coalescence made the vapor escaping much easier than it was for the larger sizes and the enhanced fluid replenishment was able to pump the cold fluid to the hot spots inside the porous covering. This led to a maximum heat transfer coefficient of values as high as 220 kW/m^{2}K at heat fluxes as low as 16.5 W/cm^2. Hence, it was concluded that the high heat transfer coefficient was achieved due to a better liquid and vapor counterflow situation inside the porous covers rather than from the extended surface effect.

Li and Peterson (2007) systematically investigated the two phase heat transfer performance of copper meshes with different geometric dimensions using DI water as the working fluid. In this study, it was concluded that the mechanisms of two phase heat transfer enhancement for copper meshes are due mainly to the extended wetted area, increased nucleation sites, intensified interaction among bubbles, and capillary evaporation. The heating surface superheat was controlled to within 15 ºC, while the heat flux reached values as high as 230 W/cm^2 for mesh with 0.57 mm^2 thickness. For the copper wire mesh of 2.3 mm thick, its CHF reached values in excess of 370 W/cm^2, or almost 2.5 times of the CHF on a plain surface when the superheat is 65ºC.

Arik, Bar-Cohen and You (2007) conducted pool boiling experiments on microporous-coated silicon heaters with FC-72 fluid. The diamond-based microporous-coated silicon heater reached a CHF of 47 W/cm2, which was a 60% enhancement compared to the CHF of a bare silicon heater. With the aid of the TME (thermal management of electronics) correlation, the effects of pressure and subcooling on CHFs have been predicted as relative identical for both the bare and microporous coated silicon heaters.

Xu et al. (2008) visualized acetone boiling on several copper foam heating surfaces. Cage bubbles—partially liquid filled bubbles—were observed in these tests. By comparing experimental results of the heat transfer coefficient and the heat flux on different PPI (Pore Per Inch) copper foams, it was demonstrated that the low PPI (large pore size) copper foam had a low resistance to the vapor release, which leads to a better heat transfer coefficient and a higher heat flux at the same superheat, in the low heat flux regime, when compared to that of a high PPI (small pore size) copper foam. The copper foam with 90 PPI generated the best two phase heat transfer performance in the high surface superheat region, extending the peak heat flux to approximately 140W/cm^2, with the assistance of the enhanced capillary force, due to its small pore size. It was concluded that the resistance to the vapor release dominates the two phase heat transfer in the low and moderate heat flux regions, while the capillary force dominates the two phase heat transfer performance of the copper foam coating in the high heat flux region. Using the same argument, it was also demonstrated that an increase in the porosity of the copper foam will decrease the heat transfer performance throughout the entire heat flux range evaluated, and that the increase of the thickness of the copper foam coating will increase the heat transfer performance in the low and middle heat flux ranges, while decreasing the heat transfer performance in the high heat flux region.

In conclusion, it was clearly shown in the previous studies that the heat transfer performance of organic fluids is relatively lower than that of water due to the lower latent heat of organic fluids, which means that even though many aspects of organic fluids make them preferable for electronics packaging components, their phase change heat transfer performance makes them less than optimal for high heat flux applications, especially when the heat flux is over 150 W/cm^2. In addition, at low heat fluxes, larger porous size structure provide better two phase heat transfer performance than the microporous structures due to the geometric effect on a single bubble departure cycle, as explained in detail by Li et al. (2010). When the heat flux reaches a relatively high level, the single bubble departure mechanism plays only a minor role in the two phase heat transfer performance, and the advantage of the large pore size structures, such as increased nucleation site density, extended surface area, and geometrical effect on the single bubble dynamics are lost. Finally, when liquid-vapor counterflow choking becomes the primary reason for the onset of CHF at high heat fluxes, special structures on porous layers can achieve much better heat transfer performance than the uniform thickness porous structures, due

Global Digital Central
ISSN: 2151-8629

to the fact that the special structures could separate the adjacent vapor columns, inhabit the hydrodynamic instability and delay the formation of the vapor blanket covering on the heating surface. A detailed summary of the experimental studies discussed above is presented in Table 1 below.

Using a novel porous structure to enhance Zuber's hydrodynamic instability limit (Zuber, 1959) and to enlarge the liquid water entrance channels to the bottom heating surface, the present investigation achieved an ultra high CHF and heat transfer coefficient for two phase heat transfer in DI water. This structure not only, enhanced the CHF value, but maintained a high heat transfer coefficient over the entire range from a low heat flux regime through the high heat flux regime.

Table 1 Summarization of pool boiling on plain surface

Author	*Porous Media*	*Fluid*	*CHF(Porous Media) W/cm^2 {CHF(Porous Media) /CHF(Plain Surface)}*	*Max. heat Transfer Coefficient (W/m^{2}K)*
Liter, Kaviany and Hwang, Min, ect	Uniform, modulated, 2D	n-Pentane	44.1—76.5 {1.8—3.11}	NA
Xu, Ji, Zhang, Liu	Foam	Acetone	80—140 {2—3.4}	20000
Li, Peterson	Mesh	Water	175—360 {1—2.1}	200000
Srinivas, Kwang	Nano Porous Media	FC-72	5 {2.5}	NA
Melendez, Reyes	Iron Wool & Stainless Steel Wool	Mixture of Water & Ethanol	NA	220000
Rainey, You	Pin Fin & Microporous Coating	FC-72	26.3--129.4 {1.4—6.9}	17500
Connor, You	Micro Porous Media	FC-72	30 {2.1}	25000
Chang, You	Micro Porous Media	FC-87&R-123	15.2--37.4 {1.2—3}	NA
Arik, Bar-Cohen, You	Diamond-based microporous-coated silicon	FC-72	19.4-47 {1.6}	NA

2. EXPERIMENTAL FACILITY AND PROCEDURE

2.1 Design and Manufacture of Copper Particle Sintered Porous Structures

Figure 1 illustrates the uniform thickness porous structure and modulated porous structures. The geometric dimensions of the modulated porous structures are illustrated in Fig. 1, as well. Three porous structure samples were tested in this investigation; one modulated porous structure and two uniform porous structures. As shown in Fig. 1 (a), the modulated porous structure has a porous base of 0.55mm. The uniform porous structures have thicknesses of 0.55 mm and 1.2 mm. The modulated porous structure was sintered on top of the heating bar assembly as illustrated in Fig. 1 (b). The four pillars of the modulated porous structures had a height of 3.6 mm which is approximately the upper limit of the Kelvin-Helmholtz instability wavelength, and a diameter of 3 mm, which is approximately the upper limit of the Rayleigh-Taylor instability wavelength (Darcy, 1856). This geometric design was selected to ensure that the neighboring vapor columns would be separated by the pillars to delay the onset of the hydrodynamic instability, which, in turn leads to improvement in the CHF. By comparing the two phase heat transfer test results of the modulated porous structures with that of the uniform porous structure of the same thickness and particle size, the contribution of the four pillars to the CHF improvement could be identified and quantified.

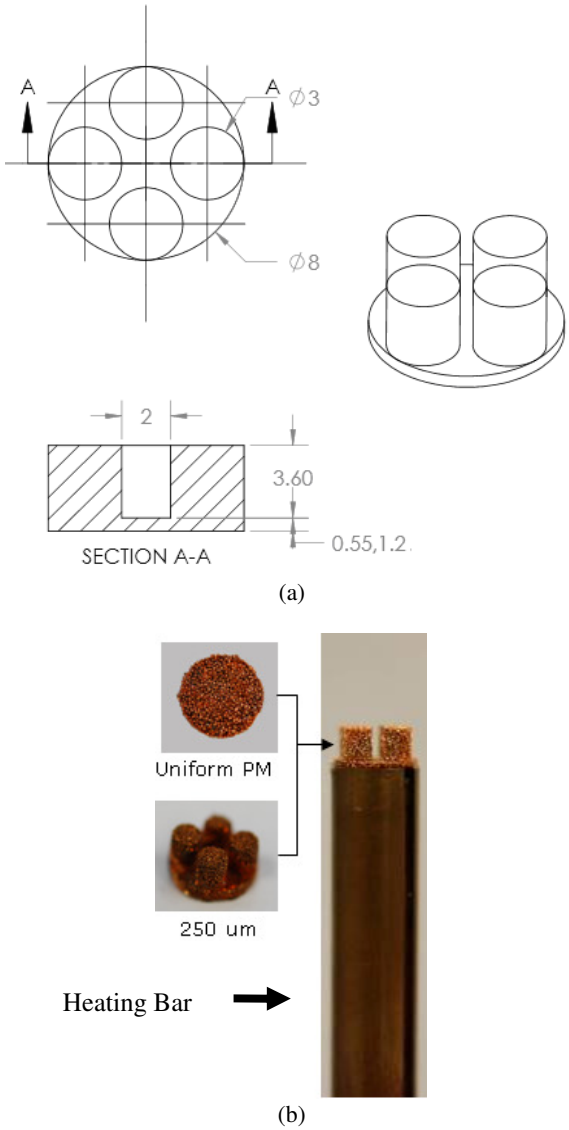

Fig. 1 Sketches of porous structures and sample pictures

The copper particle porous structures were sintered in graphite molds under high inductive heat flux in an argon environment, to prevent oxidation. The nominal diameter of the copper particles used in this experimental study was 250 μm (Acupowder International, LLC, USA). The copper particles were packed in an inverted graphite mold with the

Global Digital Central
ISSN: 2151-8629

copper heating bar pressed on top of the packed copper particles. The entire assembly was manufactured in a single sintering process to ensure uniform thermal contact between the particles and the top surface of copper heating bar. The contact resistance between the porous structure and the top surface of the copper heating bar is defined as the first contact resistance and the second was defined as that occurring between the neighboring microcopper particles inside the porous structures. In this sintering process, the pressure applied on the heating bar against the packed copper particles was carefully controlled to attain the best sintered bond and the best thermal contact inside the porous structure and between the porous structure and top surface of copper heating bar. This process negated both types of contact resistance.

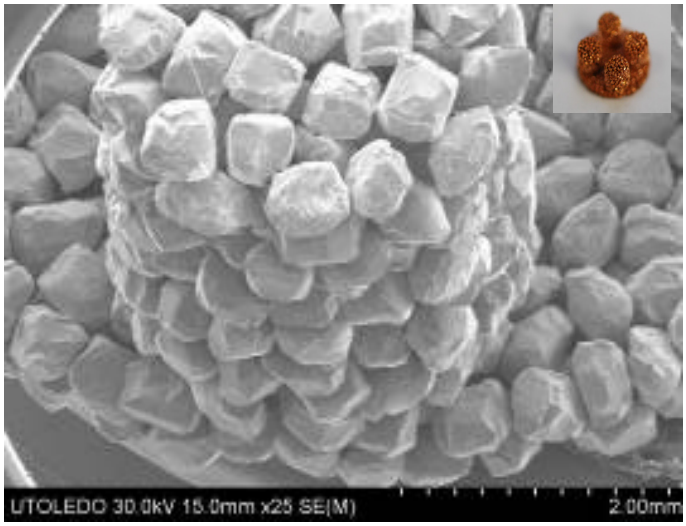

(a)

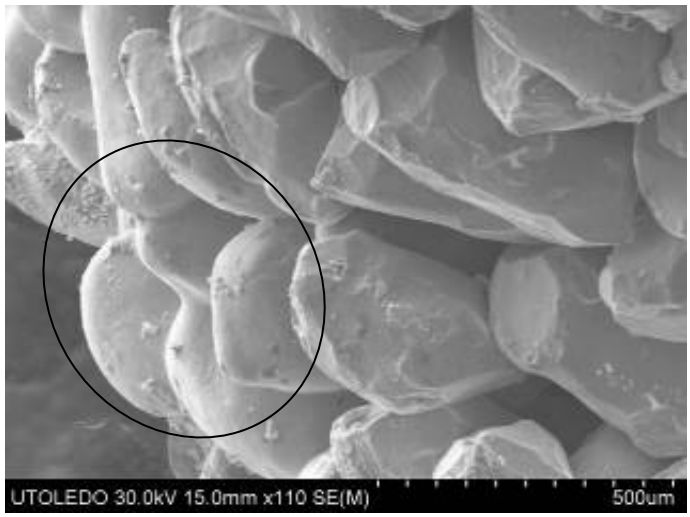

(b)

Fig. 2 SEM pictures of modulated porous structure MT-550-250

Scanning Electron Microscope (SEM) photographs of the MT-550-250 (shown in table 2) porous structure are shown in Fig. 2. As shown, the copper particles surface atoms have formed a strong bond between neighboring particles, and as proven by destructive testing of the bond strength ensured excellent sintered mechanical quality and thermal contact among the copper particles inside the porous structure. The bond between the porous structure and top surface of copper heating bar was also examined. The average void sizes of the porous structures were measured on the SEM pictures, and were found to be approximately 0.07 mm. As indicated in Fig. 3 below, bubble nucleation will begin at a very low superheat in the active nucleation cavities with sizes ranging from approximately 0.04 mm to 0.07 mm.

Examination indicated that a large percentage of the cavities inside the porous structure samples used in this investigation have a size range between 0.04 mm to 0.07 mm, indicating that the early stage nucleate boiling heat transfer coefficient will be greatly enhanced by maximizing the active nucleation site density with the sintered porous structure employed in this study.

Table 2 Parameters of tested porous structure

Test Sample No.	*Thickness (μm)*	*Porosity*	*Particle Size (μm)*
Modulated Porous media			
MT-550-250	550	27.4%	250
Uniform Porous Media			
UT-550-250	550	27.4%	250
UT-1200-250	1200	27.4%	250

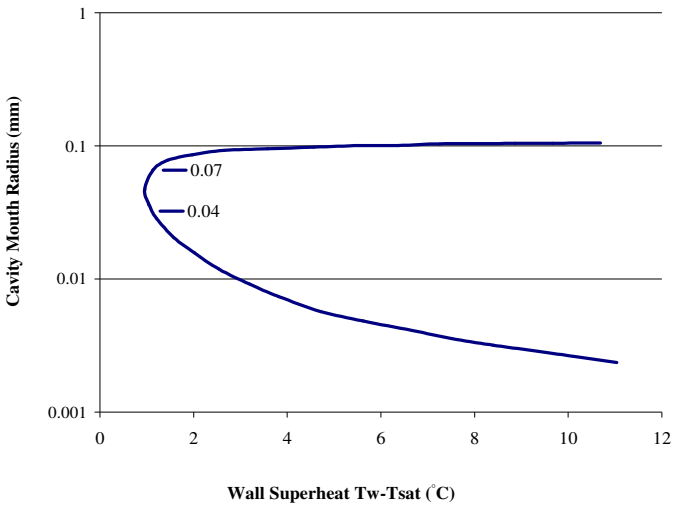

Fig. 3 Prediction of the range of active cavity sizes (Carey, 1992)

2.2 Test Facility and Measurement

As shown in Fig. 4, the test setup consists of a copper heating system, three 400W cartridge heaters, a data acquisition system, a saturate water supply system, two ceramic insulation blocks, and a glass container with a 300W guard heater. Four K-type thermocouples spaced 10 mm apart were embedded into the center of the heating bar to monitor its temperature distribution along the axis. The upper thermocouple was 1 mm beneath the interface between the heating bar and the porous structure. The water temperature within the glass container was monitored by a fifth thermocouple. The saturated degassed DI water pool boiling tests were performed on both a plain surface and the porous structures listed in Table 2. All the tests were conducted under 1 atm pressure. Temperature data collected through the thermocouples were recorded during the boiling tests and when the variation of temperature readings in all thermocouples was less than 0.1˚C over ten minutes, the data were then collected to calculate the heat fluxes and superheat temperatures.

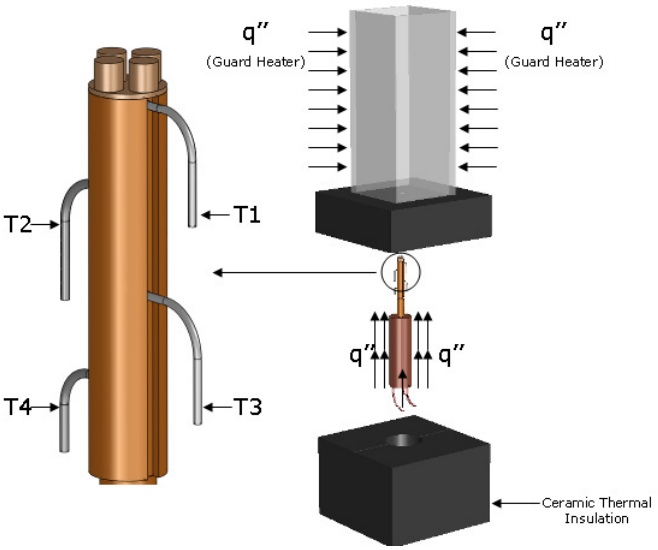

(a)

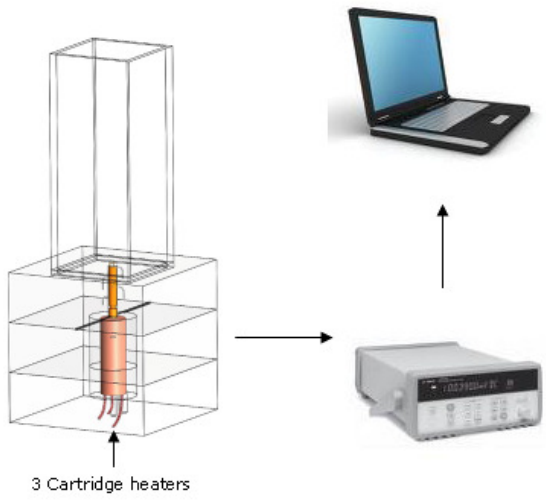

(b)

Fig. 4 Sketch of test setup system and distribution of thermocouples

2.3 Data Processing and Experimental Uncertainties

Temperature data recorded by the thermocouples were used in conjunction with Fourier's Law to calculate the heat flux (q'') passing through the porous media. Pertinent equations follow as.

$$q'' = \frac{((K_1 * (T_4 - T_3) + K_2 * (T_3 - T_2) + K_3 * (T_2 - T_1)}{3 * d} \quad (1)$$

$$T_W - T_{sat} = T_1 - T_5 - q'' * \frac{0.001}{K} \quad (2)$$

$$h = \frac{q''}{T_W - T_{sat}} \quad (3)$$

where T_x represents the thermocouple reading temperature (x=1, 2, 3, 4 and 5), T_w represents the temperature of the top surface of the heating bar, T_{sat} represents the temperature of the saturated water in the glass container, K represents the thermal conductivity of the copper heating bar, and d represents the distance between each pair of thermocouples in the heating bar. Using these values and the above equations, the heat flux, wall superheat, and heat transfer coefficient (h) were all calculated.

The uncertainty of the temperature measurement and the heat flux were ±0.5°C and ±7.5 W/cm^2 and were determined as follows. In equations (4-9), q''_{12} is the heat flux through the section of the heating bar between thermocouples 1 and 2; q''_{23} is the heat flux through the section of copper heating bar between thermocouples 2 and 3; and q''_{34} is the heat flux through the section in the copper heating bar between thermocouples 3 and 4. The variation among the values of q''_{12}, q''_{23}, and q''_{34} was consistently less than 5%.

$$q''_{mean} = \frac{q''_{12} + q''_{23} + q''_{34}}{3} \quad (4)$$

$$\Delta q''_1 = q''_{12} - q''_{mean} \quad (5)$$

$$\Delta q''_2 = q''_{23} - q''_{mean} \quad (6)$$

$$\Delta q''_3 = q''_{34} - q''_{mean} \quad (7)$$

$$\Delta q''_{max} = \max(\Delta q''_1, \Delta q''_2, \Delta q''_3) \quad (8)$$

$$q''_{error} = \frac{\Delta q''_{max}}{q''_{mean}} \quad (9)$$

Using this approach, the uncertainty of the heat transfer coefficient was found to be less than 10% as determined by equation (10).

$$dh = \frac{dq'' - hd(\Delta T)}{\Delta T} \quad (10)$$

3. RESULTS AND DISCUSSION

3.1 Pool Boiling Test on a Plain Surface

Table 3 Comparison of experimental CHF for a plain copper surface

Auracher et al., 2001	139.0 W/cm^2
Zuber, 1959	110.8 W/cm^2
Moissis & Berenson, 1962	152.4 W/cm^2
Lienhard & Dhir, 1973	126.9 W/cm^2
Li & Peterson, 2001	130.2 W/cm^2
Present Data	141.3 W/cm^2

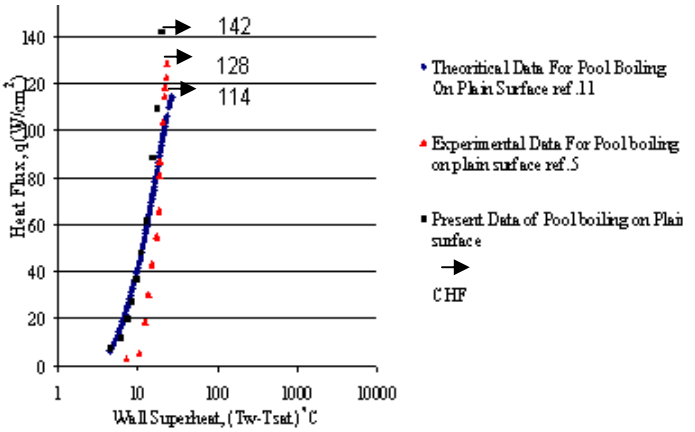

Fig. 5 Boiling curve of pool boiling on a plain surface

Tests of nucleate boiling on a plain surface were initially conducted and provided a method by which the system and procedure could be

Global Digital Central
ISSN: 2151-8629

calibrated. The results demonstrated good agreement with both the theoretical and experiment results listed in Table 3. When the heat flux reached the CHF on the plain surface, a sudden transition from nucleate boiling to film boiling was observed and the temperature readings of all four thermocouples inside the heating bar increased abruptly. Figure 5 illustrates a comparison of the current boiling data with the theoretical data and experimental data available in the literature [5]. As shown, these results confirm the approach used in the current investigation.

3.2 Nucleate Boiling Tests on Uniform Porous Structures

During the tests on the uniform porous structures (UT-550-250 and UT-1200-250) with an average pore size of approximately 70μm, both the CHF and the heat transfer coefficient demonstrated significant improvements compared to that of a plain surface. The enhancements in the CHF and heat transfer coefficient are the result of the extended heating surface effect of the uniform thickness porous structure, increased active nucleation sites, and the capillary force assisted replenishment to the bottom heating surface.

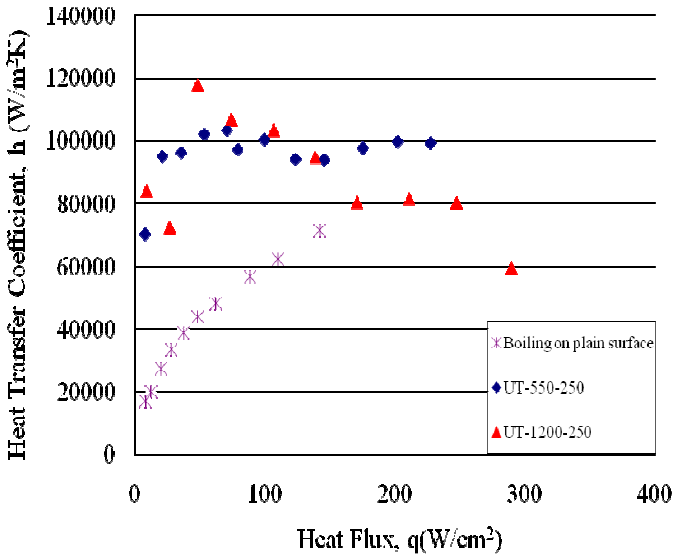

(a)

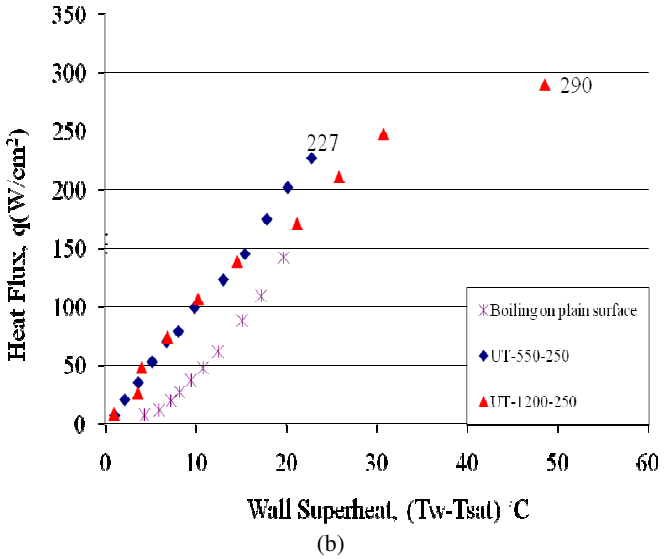

(b)

Fig. 6 Boiling curve of pool boiling on uniform porous structures

As shown, the porous structures dramatically increased the total heating surface area with very limited temperature drop from the bottom heating surface due to the minimal thicknesses. The cavities inside the uniform porous structures also offer more active nucleation sites, particularly for pore sizes of 0.07 mm. This implies that more active nucleation sites were generating single vapor bubbles at a very low superheat, which greatly enhanced the heat transfer coefficient. Bubble departure size was also influenced by the pore size.

According to previous investigations [8 and 16], the reduced bubble departure size is determined by the cavity radius and can be determined through the force balance between the buoyancy and surface tension forces. A small cavity radius means a small surface tension force at the bottom the vapor bubble, and this small surface tension force will require very little force to depart the surface. This leads to a higher heat transfer coefficient for the same heat flux and/or superheat than that obtained for a plain surface. The capillary force inside the uniform porous structures served as a pumping force to help re-wet hot spots at the bottom of the porous structures, which also greatly improved the CHF. The combination of these mechanisms led to dramatic enhancements in the CHF and heat transfer coefficients that were twice that of the plain surface as illustrated in Fig. 6.

The case of low and moderate heat flux conditions are illustrated in Fig. 6 (a) and as shown, the thicker uniform porous structure sample UT-1200-250, which was approximately twice as thick as UT-550-250, had a larger heat transfer coefficient. This is due to the fact that the thicker uniform porous structure UT-1200-250 had a much larger extended heat transfer surface area and more active nucleation sites compared to the thinner uniform porous structure UT-550-250. According to Darcy's Law [19] listed as Eq. (11), viscous drag is too small to affect the vapor escape, due to the relative low flow velocity. As a result, the thicker porous media has a better performance at low and moderate heat flux situations.

$$u = \frac{-\kappa}{\mu}\nabla P \tag{11}$$

where u is the velocity, κ is the porous permeability, μ is the viscosity, and P is the pressure.

At moderate heat fluxes, the viscous drag on the vapor flow will result in a high flow resistance to the vapor escape, due to the rapidly increased vapor flow rate. This traps vapor inside the thicker uniform porous structure (UT-1200-250) and reduces the number of active nucleation sites and reduces the two phase heat transfer coefficient of the uniform porous structures. Moreover, under high heat flux conditions, the vapor inertial energy increased so dramatically that it led to a further increase in the viscous drag. In this situation, a larger amount of vapor generated could not escape as quickly as it could in the medium heat flux situation, and the replenishment path of the liquid water and the escaping path of vapor experienced counterflow choking, which led to more localized dry-out regions inside the uniform porous structures and hence, a low heat transfer coefficient for the thick uniform porous structure when compared to the thin uniform porous structure.

Compared to the thin uniform porous structure (UT-550-250), the thick uniform porous structure (UT-1200-250) had a much higher CHF, as shown in Fig. 6(b). The explanation for this, may be based on based on Zuber's hydrodynamic instability theory [20]. According to Zuber's theory, CHF will be triggered once the vapor bubble departure velocity on the top of the uniform porous structure reaches a critical value,. The vapor critical velocity, u_v which could be calculated using Eq. 12, below

$$u_v = [\frac{\sigma m}{\rho_v}]^{\frac{1}{2}}[\frac{\rho_l}{\rho_l + \rho_v}]^{\frac{1}{2}} \tag{12}$$

where σ is the surface tension, m is the vapor mass flow rate per unit area, ρ_v is the vapor density, and ρ_l is the liquid water density.

Global Digital Central
ISSN: 2151-8629

As a result, for both the 0.55 mm and the 1.2 mm thick uniform porous structure, when the CHF is reached, the vapor bubble departure velocity should have reached the critical velocity u_v on the top of the porous structure. Following the assumption made by Zuber (1959) that, at steady-state, the two phase change will consume all of the thermal energy transferred from the heating surface, the vapor velocity generated on the bottom heating surface can be calculated based on the energy conservation in conjunction with Eq. 13

$$q' = \rho_v u_v H_{fg} A_v \tag{13}$$

where u_v is the vapor departure velocity on the top of the porous structure, H_{fg} is the latent heat of water, and A_v is the total surface area of the openings on the top of the uniform porous structure that vapor escapes through.

Using the assumptions above, Eq. 13 indicates that when the CHF has been reached, the bubble departure velocity from the top of both the thick and thin uniform porous structure is identical, while the vapor departure velocity at the bottom of the thick uniform porous structure must be higher than that observed for the thin uniform porous structure, in order to overcome the higher flow resistance inside the thick porous structure, as predicted by Darcy's Law, where the Darcy's Law points out that the thicker uniform porous structure would consume more kinetic energy of vapor flow.

Therefore, in order for the vapor velocity at the top of the thick uniform porous structure to reach the same critical vapor velocity, u_v and trigger the CHF, it must be higher than the heat flux necessary to generate a higher vapor escape velocity in order to satisfy the required critical velocity for CHF. Moreover, the CHF of the thick uniform porous structure turns out to be 290 W/cm^2, much higher than that of the thin uniform porous structure at 227 W/cm^2.

3.3 Thermal Contact Resistance Effect Tests on Two Phase Heat Transfer Performance

Figure 7 shows that two phase heat transfer performance varies greatly on the same type of modulated porous structure manufactured by different sintering processes. This variation of two phase heat transfer performance is due to the large difference of contact resistance related to different sintering processes. The better two phase heat transfer performance modulated porous structure, which had a much higher CHF and heat transfer coefficient, was sintered through the one-step manufacturing process discussed in Section 2.1.

The low performance sample was sintered in a two-step process. First, the modulated porous structure itself was sintered from the copper microparticles with a mode. Then, the sintered porous structure was sintered on the top surface of the copper heating bar. Because the mating surface of the porous structure and the top surface of the copper heating bar need extensive care to be well sintered together, more often than not, there was poor mechanical bonding and poor thermal contact between them and therefore there was a large contact resistance between the porous structure and the top surface of copper heating bar after sintering. Consequently, the heat transfer performance suffered greatly and can be observed from the photographic images and experimental data shown in Fig. 7 (a). Using a high speed CCD camera, it is clearly apparent that the vapor generated on the low performance porous structure formed a large mushroom shape, which receeded slowly and often remained on the porous structure for a short period of time, while vapor generated on the high performance porous structure had a much stronger vapor departure velocity and a very short retention period. The heat flux difference in Fig. 7 (a) at the same superheat value also illustrated that more vapor was generated, which led to the dissipation of much more thermal energy for two phase change. Figure 7 (b) demonstrated the two phase heat transfer difference of the one-step sintered and two-step sintered porous structures even more directly.

The heat transfer coefficient of the one step sintered porous structure is over two times that of the two-step sintered porous structure. This test shows that the first kind of contact resistance between the porous structure and the top surface of the copper heating bar plays a dominant role on two phase heat transfer performance. In order to achieve the lowest contact resistance, the porous structure and copper heating bar should be sintered such, that the thermal contact resistance is reduced to the greatest extent possible.

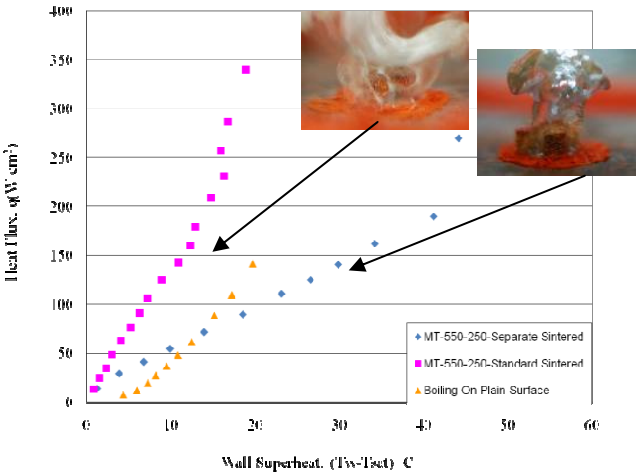

(a)

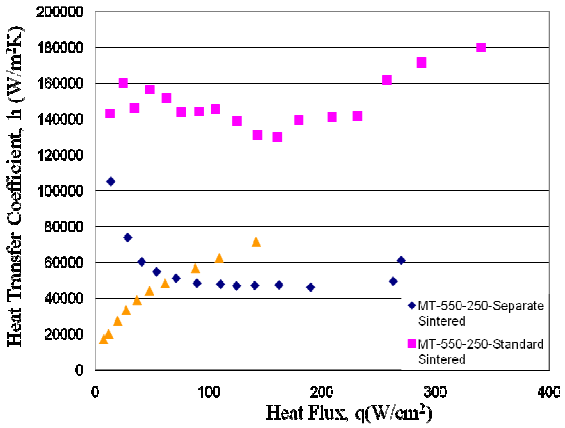

(b)

Fig. 7 Boiling curve of nucleate boiling on modulated porous structures

3.4 Heat Transfer Performance of Modulated Porous Structures

Figure 8 indicates that the modulated porous structure (MT-550-250) had an excellent two phase heat transfer performance compared to that of the thin uniform porous structures (UT-550-250) on a plain surface. The CHF of the modulated porous structure was 435 W/cm^2, while the CHFs of thin uniform porous structure and the plain surface were 227 W/cm^2 and 142 W/cm^2, respectively. The heat transfer coefficient of the modulated porous structure reached 200 kW/m^{2}K and stabilized at 180 kW/m^{2}K, while the heat transfer coefficients of the thin uniform porous structure and the plain surface were 100 kW/m^{2}K and 78 kW/m^{2}K (peak value), respectively.

The reasons for the enhanced maximum heat flux and the two phase heat transfer coefficient on the modulated porous structure MT-550-250 are believed to be (1) the increased heating surface area of the four pillars, (2) more active nucleation sites inside the modulated porous

Global Digital Central
ISSN: 2151-8629

structure, (3) enhanced both horizontal and vertical replenishments of liquid inside the porous structure, (5) and the separated vapor/liquid flow paths. As discussed in the previous section, the four pillars could also separate the neighboring vapor columns from forming a vapor blanket on the top of the porous structure. Hence, the hydrodynamic instability has been delayed and a much higher maximum high heat flux has been achieved.

As demonstrated in Fig. 8 and in Fig. 6 of section 3.2, for the uniform porous structures, the initial increase of the two phase heat transfer coefficients is due to the large number of active nucleation sites that continue to generate vapor bubbles to accommodate the heat flux increase and reduce the rate of increase of superheat temperature. Until the maximum two phase heat transfer coefficients have been reached, more vapor will be trapped inside the uniform porous structures because of the severe vapor-liquid counterflow on the top and the viscous drag inside of the uniform porous structure. The vapor blocked inside the uniform porous structure started to significantly impede the liquid replenishment to the active nucleation sites. With less vapor generated from the reduced number of active nucleation sites, the superheat temperature started to increase, much more quickly, and the two phase heat transfer coefficient begins to drop. A dynamic balance between the heat flux increase and the active nucleation site number decrease will be established at the expense of a rapid increase in the superheat temperature until the CHF has been reached.

Similarly, there are three regions in the two phase heat transfer curve of the modulated porous structure shown in Fig. 8. The first region is the two phase heat transfer coefficient increase region before the heat flux reaches 100 W/cm^2 in Fig. 8 (b) (or before the superheat temperature reaches 5 ^{o}C in Fig. 8 (a)). While in the same region, the two phase heat transfer coefficient of the thin uniform porous structures had already reached its peak and started to decline. Under low heat flux conditions (< 50 W/cm^2), the heat transfer coefficient difference between the modulated porous structure MT-550-250 and the uniform porous structure UT-550-250 is limited. In this heat flux range, the liquid replenishment to active nucleation sites is not a problem for either the uniform porous structure or the modulated porous structure. This result is opposite to the trend reported in Ref. 7, which stated that the uniform porous structure should have a higher heat transfer coefficient at low heat flux. The different findings between current work and Ref. 7 are believed to be due to differences in the modulated porous structure geometry. More specifically, it is due to the different thickness of the flat base and the different pillar shape, as well as the difference in the physical properties of the working fluids, such as latent heat, surface tension, and active nucleation cavity size range inside the porous structures. At a heat flux condition between 50 W/cm^2 and 100 W/cm^2, the porous pillars of modulated porous structure start to show one of its major roles as the liquid water replenishment path. This role minimizes the vapor/liquid counter-flow effect on liquid replenishment outside the porous structures. Unlike what occurred in the uniform porous structure cases, on the top of the uniform porous structures the vapor/liquid counter-flow constricted the access of liquid water to the uniform porous structure on top, and hence decreased the supply of liquid water to replenish the active nucleation sites inside the uniform porous structure. In the modulated porous structure case, vapor/liquid counter-flow resulted in reduced the amount of water flowing down to the porous structure base, but is of much less significance since the liquid can travel through the porous pillars and reach the active nucleation sites inside the porous base. As illustrated in Fig. 8 (b) a continuous increase of the two phase heat transfer coefficient in the first region, exists.

The dynamic balance maintained a wide range of heat flux and superheat temperature in the third region, the region of constant two phase heat transfer coefficient. The heat transfer in this region will result in the CHF value when the liquid water replenishment path through the porous pillars is blocked by the delayed hydrodynamic instability of vapor, i.e., the pillars will be covered by a vapor blanket.

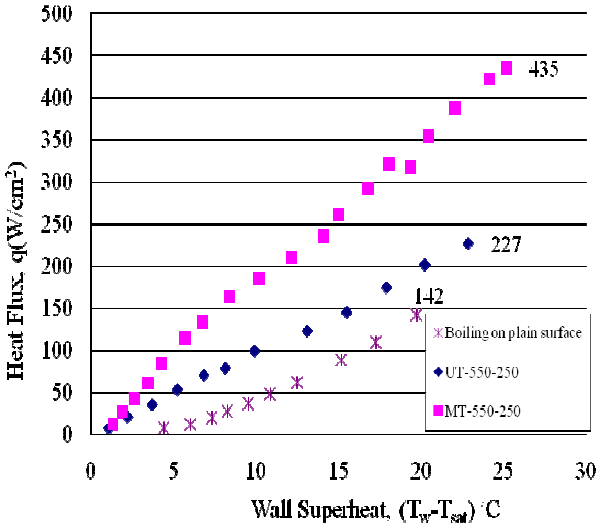

(a)

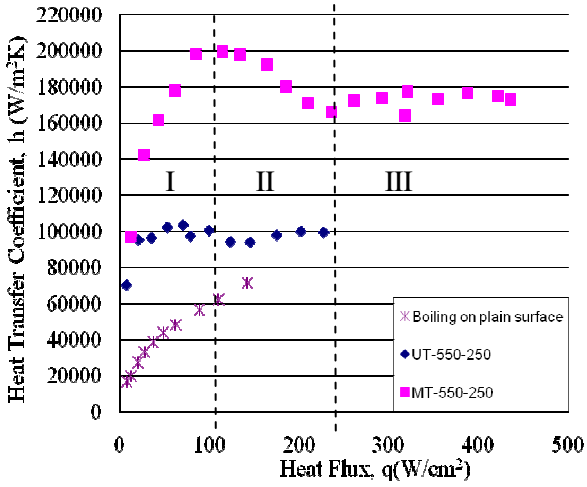

(b)

Fig. 8 Boiling curve of nucleate boiling on modulated porous structures

One conclusion of the current tests for the low heat flux condition, is that a limited number of active nucleation sites are necessary to dissipate a small amount of heat flux through the liquid/water phase change process. For this case, the four pillars do not contribute much to the actual heat transfer enhancement. However, this situation rapidly changes with increased the heat flux. For this case, the porous pillars play a much more significant role by providing liquid to the active nucleation sites in the porous base. With further increases in heat flux, more nucleation sites are deactivated by the trapped vapor and the two phase heat transfer coefficient continuously decreased until a dynamic balance was reached, the porous pillars serves as both the liquid replenishment path and separates the neighboring vapor columns to delay the onset of the hydrodynamic instability. At the end of these tests, the vapor blanket covers both the porous base and the porous pillars. The modulated porous structure delays the onset of hydrodynamic instability by separating the neighboring vapor columns with its four pillars. At the same time, the porous pillars also served as the liquid replenishing paths induced by the capillary forces, which helped to pump the liquid water to the bubble generation sites, minimizing the dry-out regions inside the porous structure. As shown in Fig. 8, the maximum heat flux achieved by the modulated porous structure MT-550-250 is over three times the CHF of a plain surface, and about two times the CHF of uniform porous structure UT-550-250.

Global Digital Central
ISSN: 2151-8629

4. CONCLUSIONS

Experimental data achieved from the calibrated test setup, indicates that a thin uniform porous structure (0.55mm thick) has a relatively constant heat transfer coefficient over the entire heat flux range evaluated. In addition, a thick porous structure (1.2mm thick) performed relatively poorly at high heat flux due to local dry out, but had a higher CHF—about twice that of a plain surface—and the maximum heat transfer coefficient at low heat flux was approximately 1.6 times than that of a plain surface. This higher CHF results from the fact that the thick porous structure consumed more kinetic energy from the escaping vapor, which caused a lower vapor column departure velocity on top of thick porous structure compared to that of the thin porous structure at the same heat flux. Consequently, when the thick porous structure had the same heat flux value as the CHF of the thin porous structure, the vapor departure velocity on top of the thick porous structure would be lower than the critical vapor velocity u_v of the thin porous structure. Therefore, the thick porous structure reaches the hydrodynamic instability later than the thin porous structure, and the CHF achieved is greater than the CHF for the thin porous structure.

The modulated porous structure exhibited excellent performance for both the CHF and heat transfer coefficient. However, due to the limitation of the heating power used in this test system and the very high heat rejection values, it was not possible to reach the CHF. In spite of this, the maximum heat flux of over 440W/cm^2 achieved in the test was over three times greater than that of a plain surface. The maximum heat transfer coefficient reached a value of 2*10^5 W/m^{2}K which is 3.6 times of that of the plain surface.

These results demonstrate that using porous pillars to separate the vapor columns from the Rayleigh-Taylor instability wavelength in the horizontal direction, and the Kelvin- Helmholtz instability wavelength in the vertical direction, the CHF can be dramatically improved. Additionally, contact resistance between the porous structure and the top surface of the copper heating bar also has a significant effect on the heat transfer performance.

ACKNOWLEDGEMENTS

The authors would like to acknowledge the generous support of The University of Toledo Startup Fund, deArce Memorial Endorsement Award, and Strategic Enhancement Award.

NOMENCLATURE

A	Surface area (m^2)
h	heat transfer coefficient (W/m^2·K)
H	latent heat of phase change (J/kg)
K	thermal conductivity (W/m·K)
m	vapor mass flow rate per unit area (kg/s·m^2)
M	molar mass (kg/kmol)
P	pressure (N/m^2)
q'	heat rate (W)
q''	heat flux (W/m^2)
T	temperature (K)
u	velocity (m/s)
Greek Symbols	
μ	viscosity (
κ	porous permeability
ρ	density (kg/m^3)
σ	surface tension (W/m$^2\cdot$K^4)
Subscripts	
error	error
fg	latent heat between liquid and vapor
l	liquid
mean	average
max	maximum
sat	saturated
v	vapor
W	top surface of the heating bar
x	*x=1, 2, 3, 4, and 5, Thermocouple number*
y	*y=1,2,3,4, 12, 23, and 34, heat flux section number*

REFERENCES

G. P. Peterson, 1994, An Introduction to Heat Pipe: Modeling, Testing and Applications, Wiley, New York

T. S. Zhao, and P. Cheng, 1998, Heat Transfer in Oscillatory Flows, in Annual Review of Heat Transfer, Chapter 7, Volume IX, Chang-Lin Tien (eds.),

A. Faghri, 1995, Heat pipe Science and Technology, Taylor & Francis, Washington, DC

P. J. Berenson, 1962, Experiments on pool boiling heat transfer, Int. J. Heat Mass Transfer 5, 985-999
doi:10.1016/0017-9310(62)90079-0

H. C. Li, T. Li, B. Kanny, 2009, Two-phase Heat Transfer Enhancement on Sintered Copper Microparticle Porous Structure Module Surface, ASME 2009 2nd Micro/Nanoscale Heat & Mass Transfer International Conference, Shanghai

H. C. Li, 2009, Experimental study on the two-phase heat transfer characteristics of copper microparticle porous structure module, 2009 ASME ASME International Mechanical Engineering Congress and Exposition, Orlando, FL

G. S. Hwang, and M. Kaviany, 2006, Critical heat flux in thin, uniform particle coatings, Int. J. Heat Mass Transfer 49, 844–849
doi:10.1016/j.ijheatmasstransfer.2005.09.020

S. G. Liter, and M. Kaviany, 2001, Pool-boiling CHF enhancement by modulated porouslayer coating: theory and experiment, Int. J. Heat Mass Transfer 44, 4287–4311
doi: 10.1016/S0017-9310(01)00084-9

D. H. Min, G. S. Hwang, Y. Usta, O.N. Cora, M. Koc, and M. Kaviany, 2009, 2-D and 3-D modulated porous coatings for enhanced pool boiling, International Journal of Heat and Mass Transfer, 52, 2607–2613
doi:10.1016/j.ijheatmasstransfer.2008.12.018

Jinliang Xu, Xianbing Ji, Wei Zhang, and Guohua Liu, 2008, Pool boiling heat transfer of ultra-light copper foam with open cells, International Journal of Multiphase Flow 34, 1008–1022
doi:10.1016/j.ijmultiphaseflow.2008.05.003

Chen Li, and G. P. Peterson, 2007, Parametric Study of Pool Boiling on Horizontal Highly Conductive Microporous Coated Surfaces, Journal of Heat Transfer 129, 1465-1475
doi:10.1115/1.2759969

Srinivas Vemuri, and Kwang J. Kim, 2005, Pool boiling of saturated FC-72 on nano-porous surface, International Communications in Heat and Mass Transfer 32, 27–31
doi:10.1016/j.icheatmasstransfer.2004.03.020

Elva Melendez and Rene Reyes, 2006, The pool boiling heat transfer enhancement from experiments with binary mixtures and porous heating covers, Experimental Thermal and Fluid Science 30, 185-192
doi:10.1016/j.expthermflusci.2005.05.005

K. N. Rainey and S. M. You, 2000, Pool boiling heat transfer from plain and microporous, square pin-finned surfaces in saturated FC-72, Journal of Heat Transfer 122 509-516
doi:10.1115/1.1288708

J. P. O'Connor and S. M. You, 1995, A painting technique to enhance pool boiling heat transfer in saturated FC-72, Journal of Heat Transfer 117 387-393
doi:10.1115/1.2822534

J. Y. Chang and S. M. You, 1997, Boiling heat transfer phenomena from microporous and porous surfaces in saturated FC-72, International Journal of Heat Mass Transfer 40, 4437-4447
doi:10.1016/S0017-9310(97)00055-0

M. Arik, A, Bar-Cohen, S. M. You, 2007, Enhancement of pool boiling critical heat flux in dielectric liquids by microporous coatings, Int. J. Heat Mass Transfer 50, 997-1009
doi:10.1016/j.ijheatmasstransfer.2006.08.005

Calvin. H. Li, Ting Li, Paul Hodgins, and G. P. Peterson, 2010, Characteristics of Pool Boiling Bubble Dynamics in Bead Packed Porous, Journal of Heat Transfer, 132, 024511

Novak Zuber, 1959, HYDRODYNAMIC ASPECTS OF BOILING HEAT TRANSFER (thesis)

Henry Darcy, 1856, Les Fontaines Publiques de la Ville de Dijon ("The Public Fountains of the Town of Dijon"), Dalmont, Paris

Van P. Carey, Liquid-Vapor Phase-Change Phenomena, 1992, Taylor & Francis, pp: 190

H. Auracher, W. Marquardt, M. Buchholz, R. Hohl, T. Luttich, and J. Blum, 2001, New Experimental Results on Steady-State and Transient Pool Boiling Heat Transfer, Therm. Sci. Eng., 9, 29-39

R. Moissis, and P. J. Berenson, 1962, On the Hydrodynamic Transitions in Nucleate Boiling, ASME 62-HT-8, Natl. Heat Transfer Conf., Houston, TX. (2)

J. H. Lienhard and V. K. Dhir, 1973, Hydrodynamic Prediction of Peak Pool-Boiling Heat Fluxes from Finite Bodies, Trans. ASME J. Heat Transfer, 95, 152-158